Local supremum/infiumum on $\mathbb{S}^2$ and mathematical morphology for images valued on the sphere

Joana Frontera-Pons and Jesus Angulo

Abstract The lack of a natural ordering on the sphere presents an inherent problem when defining morphological operators extended to the unit sphere. We analyze here the notion of averaging over the unit sphere to obtain a local origin which can be used to formulate rank based operators. The notions of local supremum and infimum are introduced, which allow to define the dilation and erosion for images valued on the sphere. The algorithms are illustrated using polarimetric images whose values are defined on the Poincaré sphere.

1 Introduction

Mathematical morphology is a well-known nonlinear approach for image processing [8]. It is based on the calculation of minimum and maximum values of local neighborhoods [11] . Computation of the supremum and infimum of a set of points requires defining an ordering relationship between them. It is obvious that there is no natural ordering on the unit (hyper-)sphere. In fact, the sphere is probably one of the more complex geometrical objects for the notion of ordering and consequently for the computation of rank values such as the supremum/infimum. Mathematical morphology operators were extended to the unit circle [5], however the generalization of such results to the unit (hyper-)sphere is not straightforward. By the way, averaging data on the sphere is also an active research [1, 3].

The values on the unit sphere may represent different kinds of physical information. In imaging applications, the most classical case is the orientation images.

Joana Frontera-Pons
SONDRA Research Alliance, Supélec, 3 rue Joliot Curie, Gif-sur-Yvette, France, e-mail: `joana.fronterapons@supelec.fr`

Jesus Angulo
CMM-Centre de Morphologie Mathématique, Mathématiques et Systèmes, MINES Paristech, 35 rue Saint-Honoré, Fontainebleau, France, e-mail: `jesus.angulo@mines-paristech.fr`

In modern medical imaging, High Angular Resolution Imaging (HARDI) produces also images with values on the sphere. Nevertheless the application domain motivating this work is the nonlinear processing of polarimetric radar data defined on spatial support.

The notion of supremum in vector spaces is usually associated to a marginal computation of maximum coordinates, which involves also a value which has maximal Euclidean distance to the origin [10, 12]. The latter considered as the smallest element of the space. A possible solution to deal with $\mathbb{S}^2$ will consist just in defining a local origin on the sphere and try after projecting on the tangent space, compute a vector-like supremum.

This is the idea which is introduced in this article. The approach induces a partial ordering "adapted" to a particular set of values on the sphere, and it is related to the definition of a barycenter, which allows defining a local Euclidean coordinate system at the tangent space.

2 Local Supremum and Infimum on $\mathbb{S}^2$

Theory and algorithms to determine supremum and infimum values for a set of points lying on $\mathbb{S}^2$ are introduced in this section. They are applied to the corresponding sup and inf operators found in the definitions of dilation and erosion, which lead to pseudo-dilation and pseudo-erosion for image valued on $\mathbb{S}^2$.

$\mathbb{S}^2$ as a Riemannian manifold

At every point $\xi_i \in \mathbb{S}^2$, with the Riemannian metric induced by the Euclidean metric on $\mathbb{R}^3$, the linear space $T_{\xi_i}\mathbb{S}^2$ tangent to the sphere is given by the exponential map $\exp_{\xi_i}(v_j)$ at ξ_i, such that $T_{\xi_i}\mathbb{S}^2 = \left\{ v_j \in \mathbb{R}^3 \ : \ v_j^T \cdot \xi_i = 0 \right\}$, where the vector point is $v_j = \left(v_{1,j}, v_{2,j}, v_{3,j}\right)$. We note also that the exponential map $\exp_\xi$ is defined by the correspondence $v \mapsto \gamma_v(1)$, where $\gamma_v : t \mapsto \gamma_v(t)$ is the unique geodesic satisfying for initial point $\gamma_v(0) = \xi$ and initial tangent vector $\dot{\gamma}(0) = v$, provided $\gamma_v(t)$ extends at least to $t = 1$.

Fréchet - Karcher barycenter on $\mathbb{S}^2$.

The Fréchet mean is defined as the value minimizing the sum of squared distances along geodesics on Riemannian manifolds [4, 6], i.e., for a given set of points $R = \{\xi_i\}_{i=1}^N$ on the sphere, we have

$$\mu^\circ(R) = \underset{\xi \in \mathbb{S}^2}{\arg\min} \sum_{i=1}^{N} d(\xi_i, \xi_k)^2 \tag{1}$$

The problem of computation of the Fréchet mean on the sphere μ° is usually solved using a gradient descent method as proposed by Karcher [6]. Some of the properties of unicity were particulary studied in [1].

The method to estimate the Fréchet mean on a sphere consists first projecting the points $\xi_i \in \mathbb{S}^2$ onto a tangent plane $T_{\mathbf{y}_t}\mathbb{S}^2$ at an initial point $\mathbf{y}_t \in \mathbb{S}^2$ by an inverse projection

$$\nu_i = \exp_{\mathbf{y}_t}^{-1}(\xi_i) \tag{2}$$

where $\nu_i \in \mathbb{R}^3$. Then, an expectation $\mathbb{E}[\cdot]$ is calculated on the tangent plane $T_{\mathbf{y}_t}\mathbb{S}^2$ and projected back onto $\mathbb{S}^2$ by a projection $\exp_{\mathbf{y}_t}$, i.e.,

$$\mathbf{y}_{t+1} = \exp_{\mathbf{y}_t}\left(\mathbb{E}\left[\{\nu_\mathbf{i}\}_{i=1}^N\right]\right) \tag{3}$$

where $\mathbb{E}\left[\{\nu_\mathbf{i}\}_{i=1}^N\right] = \left(\frac{1}{N}\sum_1^N \nu_{1,i}, \frac{1}{N}\sum_1^N \nu_{2,i}, \frac{1}{N}\sum_1^N \nu_{3,i}\right)$. See Fig. 1.

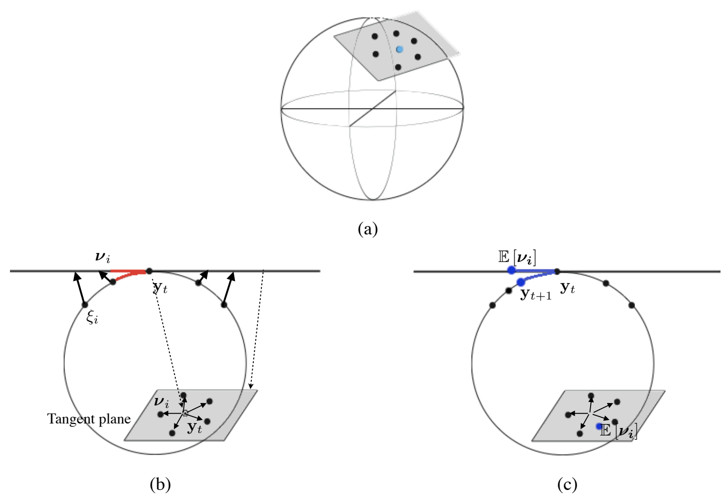

Fig. 1 Iterative method for computing the Fréchet-Karcher mean for data on the sphere: (a) Tangent space of $\mathbb{S}^2$ at green point. (b) and (c) barycenter on $\mathbb{S}^2$ using exponential and logarithmic maps.

For the unit sphere $\mathbb{S}^2$, with the Riemannian metric induced by the Euclidean metric on $\mathbb{R}^3$, the inverse exponential map (or logarithmic map) is given by [2]

$$\exp_{\mathbf{y}}^{-1}(\xi) = [1-(\mathbf{y}\cdot\xi)^2]^{-1/2}(\xi-(\mathbf{y}\cdot\xi)\mathbf{y})\arccos(\mathbf{y}\cdot\xi) \tag{4}$$

where $\mathbf{y}, \xi \in \mathbb{S}^2$. The explicit expression for the exponential map is [2]

$$\exp_{\mathbf{y}}(\nu) = \cos(\|\nu\|)\mathbf{y} + \sin(\|\nu\|)\frac{\nu}{\|\nu\|} \tag{5}$$

where $\nu \in T_{\mathbf{y}}\mathbb{S}^2$ and $\nu \neq (0,0,0)$.

Using t as an iteration index, Eq. (2) and (3) leads to a gradient descent iterative algorithm Choosing an appropriate starting point $\mathbf{y}_0$ the algorithm converges within a few iterations to the Fréchet mean: $\mathbf{y}_{t=T} = \mu^\circ(R)$ such that $\mathbf{y}_{T+1} = \mathbf{y}_T$.

Supremum.

Let $R = \{\xi_i\}_{i=1}^N$ be a set of points lying on the sphere surface. First, the Fréchet mean of the set is computed, as explained in previous section : $\bar{\xi} = \mu^\circ(R)$.

Considering this center as the local origin of set R, we use it to carry out a rotation on $\mathbb{S}^2$ of each point belonging to the set R. The barycenter is moved to the "north pole", $\mathbf{N} = (0,0,1)$, and this translation completely describes the axis and the angle needed to determine the rotation matrix $\mathscr{M}_\mathbf{N}(\bar{\xi})$, which is then applied to all the points for the points of R:

$$\xi_i \mapsto \tilde{\xi}_i = \mathscr{M}_\mathbf{N}(\bar{\xi}) \cdot \xi_i^T \quad \forall \xi_i \in R \tag{6}$$

where T is the transpose operator and ˜ indicates the location coordinates once rotated. Therefore, all $\tilde{\xi}_i \in \tilde{R}$ and $\tilde{\bar{\xi}} = (0,0,1)$, the previously computed Fréchet mean, are placed around $\mathbf{N}$, preserving the same configuration they had, see Fig. 4.

Next step, all $\tilde{\xi}_i \in \tilde{R}$ will be projected to the space tangent at $\mathbf{N}$, denoted $T_\mathbf{N}\mathbb{S}^2$, using the expression referred in Eq. (4). Let us denote by $\nu_i = (\nu_{1,i}, \nu_{2,i}, \nu_{3,i})$ are the projected points on $T_\mathbf{N}\mathbb{S}^2$:

$$\nu_i = \exp^{-1}_{\tilde{\bar{\xi}}}(\tilde{\xi}_i) \tag{7}$$

Thus, having $\mathbf{N} = (0,0,1)$ as the projection point leads to a tangent plane contained in $\mathbb{R}^2$, i.e., $T_\mathbf{N}\mathbb{S}^2 \subset \mathbb{R}^2$ such that $\nu_{3,j} = 0, \forall j$.

Our aim is to endow the Euclidean space $T_\mathbf{N}\mathbb{S}^2 \subseteq \mathbb{R}^2$ with an order structure. The natural choice involves to consider $T_\mathbf{N}\mathbb{S}^2$ as vector lattice (or Riesz space), such that given the partial ordering $\leq$ we have: (a) if $\mathbf{x}$, $\mathbf{y}$, $\mathbf{z} \in T_\mathbf{N}\mathbb{S}^2$ and $\mathbf{x} \leq \mathbf{y}$ then $\mathbf{x} + \mathbf{z} \leq \mathbf{y} + \mathbf{z}$; (b) if $\mathbf{x}$, $\mathbf{y} \in T_\mathbf{N}\mathbb{S}^2$, $0 \leq \alpha \in \mathbb{R}$ and $\mathbf{x} \leq \mathbf{y}$ then $\alpha\mathbf{x} \leq \alpha\mathbf{y}$. More precisely, if we consider the positive cone of the vector lattice given by $[T_\mathbf{N}\mathbb{S}^2]_+ = \left\{\mathbf{x} = (x_1, x_2) \in T_\mathbf{N}\mathbb{S}^2 \, : \, x_1 \geq 0, \ x_2 \geq 0, \right\}$, the natural vector ordering $\leq$ is defined in the sense that $\mathbf{x} \leq \mathbf{y} \Leftrightarrow (\mathbf{y} - \mathbf{x}) \in [T_\mathbf{N}\mathbb{S}^2]_+$.

By construction of this tangent space, with the origin associated to the barycenter, the coordinates $\nu_i = (\nu_{1,i}, \nu_{2,i}, 0)$ are positive and negative values and the partial ordering associated to the Cartesian product space $\mathbb{R} \times \mathbb{R}$ does not make sense. Therefore, given two vectors $\mathbf{x}$, $\mathbf{y} \in T_\mathbf{N}\mathbb{S}^2$, such that $\mathbf{x} = (x_1, x_2)$, we introduce the following *symmetric vector partial ordering*:

$$\mathbf{x} \preceq^{\mathrm{box}} \mathbf{y} \Leftrightarrow \begin{cases} 0 \leq x_1 < y_1 \text{ and } 0 \leq x_2 < y_2 \\ 0 \leq x_1 < y_1 \text{ and } y_2 < x_2 < 0 \\ y_1 < x_1 < 0 \text{ and } 0 \leq x_2 < y_2 \\ y_1 < x_1 < 0 \text{ and } y_2 < x_2 < 0 \end{cases} \tag{8}$$

We notice that this is only a partial but not total ordering; e.g., $\nu_1 = (3, -1, 0)$ and $\nu_2 = (-2, -1, 0)$ are not comparable. Or in other words, only vector lying in the same quadrant of $T_\mathbf{N}\mathbb{S}^2$ are comparable.

Endowed with the partial ordering $\preceq^{\text{box}}$, $T_{\mathbf{N}}\mathbb{S}^2$ is a real partially ordered vector space where the *symmetric vector supremum* is defined by the the 4-tuple

$$v_{sup}^{\text{box}} = \bigvee_{1\le i\le N}^{\text{box}} v_i = \{v_{sup}^{1,\square}, v_{sup}^{2,\square}, v_{sup}^{3,\square}, v_{sup}^{4,\square}\} \tag{9}$$

with the four values are obtained as the minimum and maximum values of each of the coordinates for both axes, and the combinations between them, i.e.,

$$v_{sup}^{1,\square} = (\bigvee_{1\le i\le N} v_{1,i}, \bigvee_{1\le i\le N} v_{2,i}) \ , \ v_{sup}^{2,\square} = (\bigwedge_{1\le i\le N} v_{1,i}, \bigwedge_{1\le i\le N} v_{2,i}),$$
$$v_{sup}^{3,\square} = (\bigvee_{1\le i\le N} v_{1,i}, \bigwedge_{1\le i\le N} v_{2,i}) \ , \ v_{sup}^{4,\square} = (\bigwedge_{1\le i\le N} v_{1,i}, \bigvee_{1\le i\le N} v_{2,i})$$

which correspond to the corners of the smallest box that may contain these points in $T_{\mathbf{N}}\mathbb{S}^2$, see Fig. 2.

We can easily see that the symmetric vector supremum commutes with the "union", i.e., let $\{\mathbf{u}_k\}_{k=1}^K$ and $\{\mathbf{v}_l\}_{l=1}^L$ two set of vectors lying in $T_{\mathbf{N}}\mathbb{S}^2$ and $\mathbf{u}_{sup}^{\text{box}}$ and $\mathbf{v}_{sup}^{\text{box}}$ their respective symmetric vector supremum, we have $\bigvee^{\text{box}}\left\{\{\mathbf{u}_k\}_{k=1}^K \cup \{\mathbf{v}_l\}_{l=1}^L\right\} = \left\{\bigvee_{1\le k\le K}^{\text{box}} \mathbf{u}_k\right\} \vee^{\text{box}} \left\{\bigvee_{1\le l\le L}^{\text{box}} \mathbf{v}_l\right\} = \mathbf{u}_{sup}^{\text{box}} \vee^{\text{box}} \mathbf{v}_{sup}^{\text{box}} = \bigvee^{\text{box}}\left\{\mathbf{u}_{sup}^{\text{box}} \cup \mathbf{v}_{sup}^{\text{box}}\right\}$. Geometrically, we can say that the supremum of two boxes is defined the minimal box containing both.

Endowed with the supremum $\bigvee^{\text{box}}$ $T_{\mathbf{N}}\mathbb{S}^2$ is an upper semilattice: a partially ordered set which has a least upper bound (i.e., a supremum) for any nonempty finite subset.

Obviously, for our purpose of data processing valued on $\mathbb{S}^2$, a 4-tuple cannot be naturally manipulated. Therefore, we propose to define as *asymmetric vector supremum* the corner of the box which is the furthest from $\bar{\tilde{\xi}}$. As $\bar{\tilde{\xi}}$ in tangent space $T_{\mathbf{N}}\mathbb{S}^2$ corresponds to the origin $(0,0)$, it is equivalent to say that v_{sup} is the corner of the box having the largest norm, i.e.,

$$v_{sup} = \curlyvee_{1\le i\le N} v_i = \arg\max_{1\le j\le 4} \|v_{sup}^{j,\square}\| \tag{10}$$

Without going into details, one can check that underlying the asymmetric vector supremum $\curlyvee$ we have the following vector partial ordering

$$\mathbf{x} \preceq \mathbf{y} \Leftrightarrow |x_1| \le |y_1| \quad \text{and} \quad |x_2| \le |y_2|$$

Nevertheless the asymmetrization of the box supremum leads to a theoretically weaker framework since for instance the vector supremum $\curlyvee$ does not commute with the union.

Now, v_{sup} is projected back to the sphere, according to Eq. (5):

$$\tilde{\xi}_{sup} = \exp_{\bar{\tilde{\xi}}}(v_{sup}) \tag{11}$$

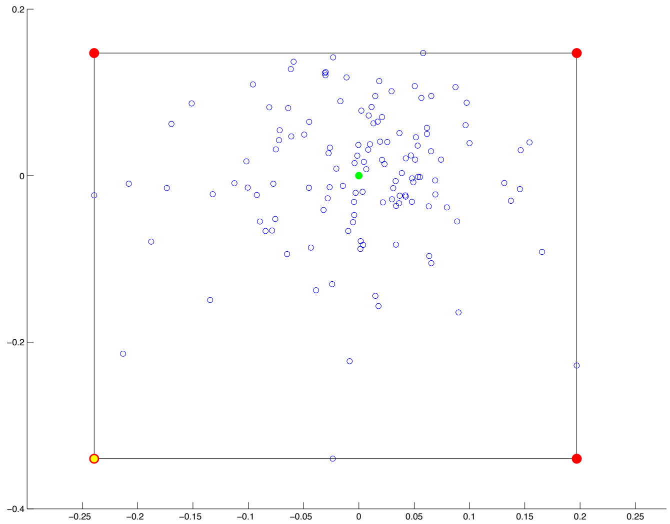

Fig. 2 Tangent plane $T_{\mathbf{N}}\mathbb{S}^2$, with all the projected points v_i. We note that $\tilde{\bar{\xi}}$, in green, is found at the origin. The red dots are the 4-tuple supremum $v_{sup}^{\mathrm{box}} = \left\{v^{j,\square}\right\}_{j=1}^{4}$, and the yellow one is the furthest from the origin v_{sup}.

and finally moved to its corresponding location by reversing the rotation:

$$\overset{\circ}{\sup_{\bar{\xi}}}\left[\{\xi_i\}_{i=1}^{N}\right] = \mathscr{M}_{\mathbf{N}}(\bar{\xi})^T \cdot \tilde{\xi}_{sup}^T \tag{12}$$

An example of the complete algorithm is given in Fig. 4.

Infimum. The method proposed to calculate the infimum is similar to the one presented for the supremum. In fact, we will introduce a *duality* in $T_{\mathbf{N}}\mathbb{S}^2$ which is defined by the *complement of the coordinates*:

$$v_i = (v_{1,i}, v_{2,i}, 0) \mapsto \complement v_i = \left(sign(v_{1,i}) \cdot (M - |v_{1,i}|), sign(v_{2,i}) \cdot (M - |v_{2,i}|), 0\right)$$

where M is the bound for both coordenates values on the tangent space $T_N\mathbb{S}^2$.
We start by the same steps as for the supremum: after computing the Fréchet mean Eq.(3), and performing the rotation of the set Eq.(6), all $\tilde{\xi}_i \in \tilde{R}$ are projected to the plane tangent at $\mathbf{N}$ using Eq.(7).

Now, the complement coordinates of each v_i lying on $T_N\mathbb{S}^2$ are computed to obtain the set of points given by

$$\theta_i = \complement v_i = \left(sign(v_{1,i}) \cdot (M - |v_{1,i}|), sign(v_{2,i}) \cdot (M - |v_{2,i}|), 0\right) \tag{13}$$

Computing the maximum and minimum for the complemented coordinates $\theta_{1,i}$ and $\theta_{2,i}$, $i = 1, \cdots, N$, it is obtained, as for the supremum, a box defining the symmetric

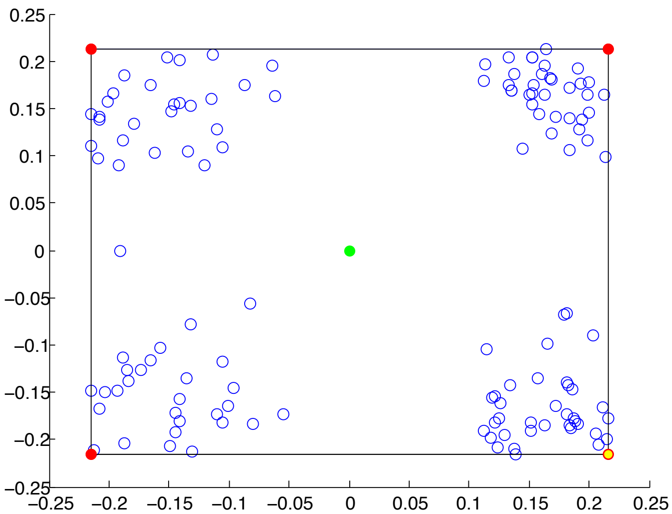

Fig. 3 Complement plane from tangent plane $T_{\mathbf{N}}\mathbb{S}^2$. The points are displayed once their coordinates have been complemented, θ_i, $\tilde{\tilde{\xi}}$ in green is found at the origin (without inversion since its inversion correspond to the infinity). The four red dots are the candidates to infimum and in yellow, the chosen one.

vector infimum of the set of initial points points, i.e.,

$$v_{inf}^{\text{box}} = \bigwedge_{1\leq i\leq N}^{\text{box}} v_i = \complement\left[\bigvee_{1\leq i\leq N}^{\text{box}} \theta_i\right] = \{\complement\theta_{sup}^{1,\square}, \complement\theta_{sup}^{2,\square}, \complement\theta_{sup}^{3,\square}, \complement\theta_{sup}^{4,\square}\} \tag{14}$$

where

$$\theta_{sup}^{1,\square} = \left(\bigvee_{1\leq i\leq N} \theta_{1,i}, \bigvee_{1\leq i\leq N} \theta_{2,i}\right), \quad \theta_{sup}^{2,\square} = \left(\bigwedge_{1\leq i\leq N} \theta_{1,i}, \bigwedge_{1\leq i\leq N} \theta_{2,i}\right)$$
$$\theta_{sup}^{3,\square} = \left(\bigvee_{1\leq i\leq N} \theta_{1,i}, \bigwedge_{1\leq i\leq N} \theta_{2,i}\right), \quad \theta_{sup}^{4,\square} = \left(\bigwedge_{1\leq i\leq N} \theta_{1,i}, \bigvee_{1\leq i\leq N} \theta_{2,i}\right)$$

Endowed with the infimum $\bigwedge^{\text{box}} T_{\mathbf{N}}\mathbb{S}^2$ is an lower semilattice: a partially ordered set which has a greatest lower bound (i.e., a infimum) for any nonempty finite subset. Geometrically the box associated to the infimum corresponds just to the one containing the origin without including the asymmetric vector infimum.

Again, to solve the lack of tractability of a 4-tuple, we propose to select as infimum the corner of the inverted box being furthest from the Fréchet mean, i.e.,

$$\theta_{sup} = \arg\max_{1\leq j\leq 4} \|\theta_{sup}^{j,\square}\| \tag{15}$$

The coordinates of the point θ_{inf} are reinverted to obtain the *asymmetric vector infimum* in the original tangent space $T_N\mathbb{S}^2$:

$$v_{inf} = \curlywedge_{1\leq i\leq N} v_i = \complement\theta_{sup} = \big(sign\theta_{1,sup}\cdot(M-|\theta_{1,sup}|), sign\theta_{2,sup}\cdot(M-|\theta_{2,sup}|),,0\big)$$

and then, v_{inf} on $T_N\mathbb{S}^2$ is projected back onto the sphere:

$$\tilde{\xi}_{inf} = \exp_{\tilde{\bar{\xi}}}(v_{inf}) \tag{16}$$

In the last step, the infimum for R is obtained once the rotation is undone:

$$\overset{\circ}{\underset{\bar{\xi}}{\inf}}\left[\{\xi_i\}_{i=1}^N\right] = \mathscr{M}_{\mathbf{N}}(\bar{\xi})^T\cdot\tilde{\xi}_{inf}^T \tag{17}$$

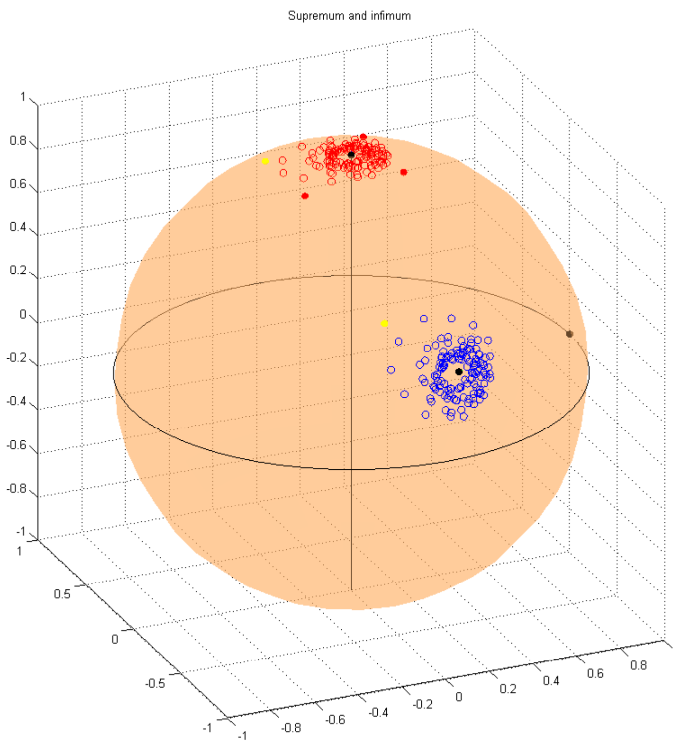

Fig. 4 Original set R of points (in blue), and its Fréchet mean in green. The result of the rotation of the set to $\mathbf{N}$ (in red), and how v_{sup} is projected back to the sphere and the rotation is reversed, in yellow the value of the supremum and in black the value of the infimum.

Definition of sup/inf-based operators. Given a 2D image valued on the sphere $f(x,y)\in\mathscr{F}(E,\mathbb{S}^2)$, $(x,y)\in E\subset\mathbb{Z}^2$, we introduce the *flat pseudo-dilation on the* *sphere* as the operator defined by

$$\begin{cases} \delta^{\circ}_{W,B}(f)(x,y) = \left\{ \sup^{\circ}_{\bar{\xi}} \left[f(u,v) = \xi_j \right], (u,v) \in B(x,y) \right\} \\ \text{with } \bar{\xi} = \mu^{\circ} \left(\left[f(n,m) = \xi_i \right] \right), (n,m) \in W(x,y) \end{cases} \tag{18}$$

where B defines the shape of the structuring element and W is the window used for computing the Fréchet mean $\bar{\xi}$. Similarly, the *flat pseudo-erosion on the sphere* is defined by

$$\begin{cases} \varepsilon^{\circ}_{W,B}(f)(x,y) = \left\{ \inf^{\circ}_{\bar{\xi}} \left[f(u,v) = \xi_j \right], (u,v) \in \check{B}(x,y) \right\} \\ \text{with } \bar{\xi} = \mu^{\circ} \left(\left[f(n,m) = \xi_i \right] \right), (n,m) \in W(x,y) \end{cases} \tag{19}$$

They are referred as "pseudo-dilation" (resp. "pseudo-erosion") because, although its behavior is intuitively coherent with the classical dilation (resp. erosion), they are not fully equivalent. More precisely, the distributivity and associativity properties are not satisfied for the operators (18) and (19). These limitations are well known for the "locally adaptive" operators [7]; we note that here the adaptavility appears in the computation of the local origin, which involves a supremum/infimum associated to tangent space at this local origin.
We need to use two different sizes for W and B to solve the instability of the Fréchet mean in neighborhoods near the edge of an object. Hence, the size of the window for the Fréchet mean computation W is increased respect to B, i.e., $B \subset W$, to make it more robust to the variability of the barycenter near edges. By this technique we can guarantee that the supremum/infimum for two close pixels is computed in the same tangent space, that is, the origin on the sphere will be the same.

3 Application to morphological processing of images valued on $\mathbb{S}^2$

Using the pseudo-dilation and pseudo-erosion on the sphere as basic bricks, other derived morphological operators can be extended to images valued on the sphere.

Gradient on the sphere. Using the proposed formulations on the sphere for pseudo-dilation (18) and pseudo-erosion (19), we define the *morphological gradient on the sphere* of image $f \in \mathscr{F}(E, \mathbb{S}^2)$ as their difference image:

$$g^{\circ}_{W,B}(f)(x,y) = d\left(\delta^{\circ}_{W,B}(f)(x,y), \varepsilon^{\circ}_{W,B}(f)(x,y)\right), \tag{20}$$

where $d(\xi_i, \xi_j)$ is the Riemannian distance on $\mathbb{S}^2$.

Pseudo-opening and pseudo-closing on the sphere. In mathematical morphology, opening and closing are two key transformations for filtering purposes, both derived from erosion and dilation by their direct products. Now, using the corresponding expressions detailed on the sphere, we shall define the *flat pseudo-opening on the sphere* of an image $f \in \mathscr{F}(E, \mathbb{S}^2)$ as the flat pseudo-dilation (18) applied on the resulting pseudo-erosion (19) of the original image f, i.e.,

$$\gamma^{\circ}_{W,B}(f) = \delta^{\circ}_{W,B}\left(\varepsilon^{\circ}_{W,B}(f)\right). \tag{21}$$

Similarly, the *flat pseudo-closing on the sphere* is defined as

$$\varphi^{\circ}_{W,B}(f) = \varepsilon^{\circ}_{W,B}\left(\delta^{\circ}_{W,B}(f)\right). \tag{22}$$

The interpretation of these operators is exactly the same as for the opening/closing of grey-level images: opening removes objects from the foreground smaller than the structuring element and closing eliminates small holes in the background.

Top-hat on the sphere. Once the pseudo-opening and pseudo-closing on the sphere have been well-defined, we can also generalize the corresponding residue-based operators. Indeed the *white top-hat on the sphere* is the residue between the original image and its pseudo-opening transformation:

$$\rho^{+,\circ}_{W,B}(f)(x,y) = d\left(f(x,y), \gamma^{\circ}_{W,B}(f)(x,y)\right). \tag{23}$$

Similarly, the *black top-hat on the sphere* is the residue between the original image and its pseudo-closing. As for the grey-level case, the white (resp. black) top-hat allows extracting the image structures which have been removed by the opening (resp. the closing).

For the examples given in Fig. 5, each pixel denotes a polarization state (ie., a point lying on the sphere surface) or more generally an ellipsoid describing the distribution of gradient directions. We point out that the performance of the described operators remains consistent with the definitions for a grey-level image.

4 Conclusions and perspectives

We have explored a novel approach to the computation of supremum and infimum of a set of points on $\mathbb{S}^2$, which is based on the notion of local origin to obtain the best tangent space where the supremum and infimum are computed as a vector notion. This methodology seems interesting from a practical viewpoint since the obtained morphological filters produce useful results. There are some questions which should be explored in detail in subsequent studies. On the one hand, it should be proved that this local approach is more appropriate than a global one, typically computing the supremum and infimum in the space associated to the stereographic projection. On the other hand, there are some limited invariance properties of the supremum and infimum which are due to the computation in a rectangular box. It seems more interesting to consider a Euclidean ball (i.e., the supremum can be the point of the minimum enclosing ball which have the largest norm). A deeper study on the mathematical properties of the proposed pseudo-dilation and pseudo-erosion is also required.

References

1. S.R. Buss, J.P. Fillmore. *Spherical averages and applications to spherical splines and interpolation.* ACM Transactions on Graphics, 20: 95–126, 2001.
2. P.T. Fletcher, S. Venkatasubramanian, S. Joshi. *Robust Statistics on Riemannian Manifolds via the Geometric Median.* In Proceedings of CVPR'08, 2008.
3. S. Fiori. *On vector averaging over the unit hypersphere.* Digital Signal Processing, 19:715–725, 2009.
4. M. Fréchet. *Les élements aléatoires de nature quelconque dans un espace distancié.*Ann. Inst. H. Poincaré, 10: 215–310, 1948.
5. A. Hanbury, J. Serra. *Morphological Operators on the Unit Circle.* IEEE Transactions on Image Processing, 10(12):1842–1850, 2001.
6. H. Karcher. *Riemann center of mass and mollifier smoothing.* Communications on Pure and Applied Mathematics, 30: 509–541, 1997.
7. J. Roerdink. *Adaptivity and group invariance in mathematical morphology.* In Proc. of IEEE International Conference on Image Processing (ICIP'09), pp. 2253–2256, 2009.
8. J. Serra. *Image Analysis and Mathematical Morphology, Vol I.* Academic Press, NY, London, 1982.
9. J. Serra. *Image Analysis and Mathematical Morphology Vol.2: Theoretical Advances.* Academic Press, NY, London, 1988.
10. J. Serra. *Anamorphoses and Function Lattices (Multivalued Morphology).* In (Dougherty, Ed.) Mathematical Morphology in Image Processing, Marcel-Dekker, 483–523, 1992.
11. P. Soille. *Morphological Image Analysis.* Springer-Verlag, Berlin, 1999.
12. S. Velasco-Forero, J. Angulo. *Supervised ordering in R^n: Application to morphological processing of hyperspectral images.* IEEE Transactions on Image Processing, 20(11): 3301–3308, 2011.
13. Y. Wang, C. Han. PolSAR Image Segmentation by Mean Shift Clustering in the Tensor Space. In *Acta Automatica Sinica* 36: 798–806, 2010.
14. http://www.ceremade.dauphine.fr/ peyre/matlab/diffc/content.html#3

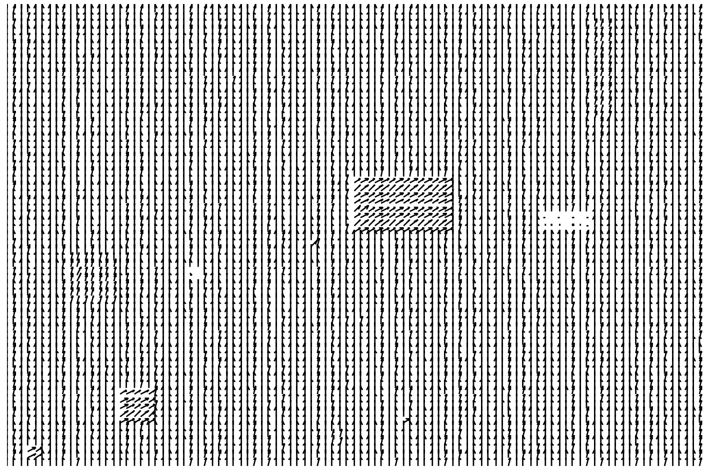

(a) $f(x,y)$

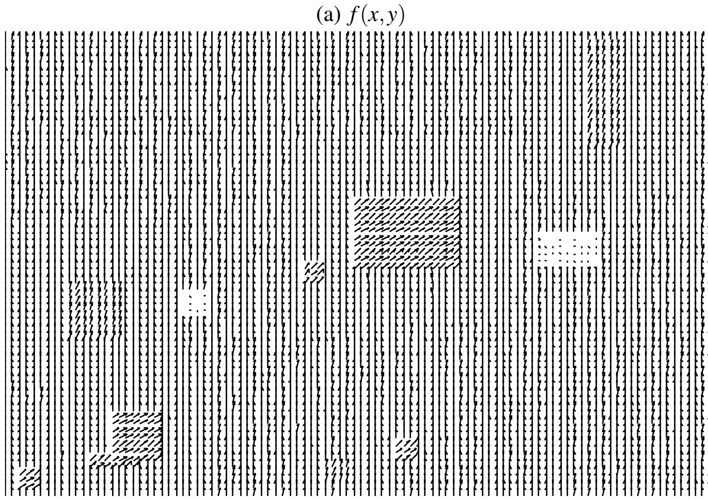

(b) $\delta^{\circ}_{W,B_5}(f)(x,y)$

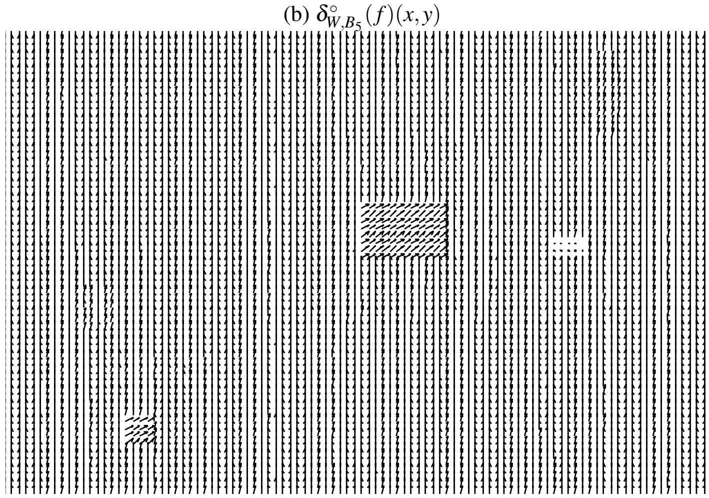

(c) $\varepsilon^{\circ}_{W,B_5}(f)(x,y)$

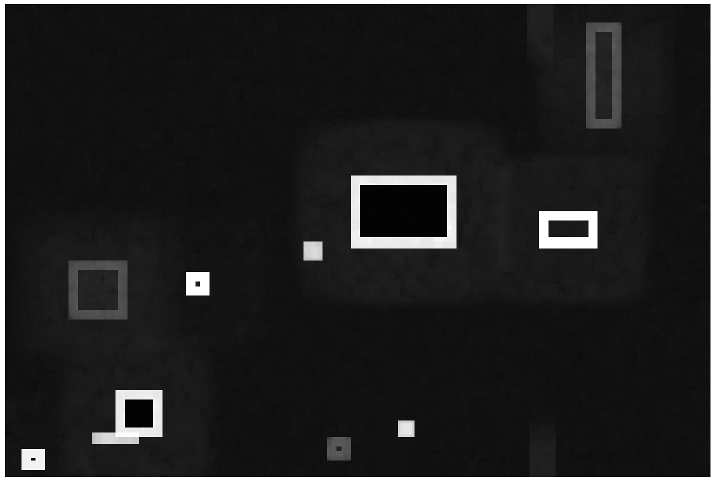

(d) $g^{\circ}_{W,B_5}(f)(x,y)$

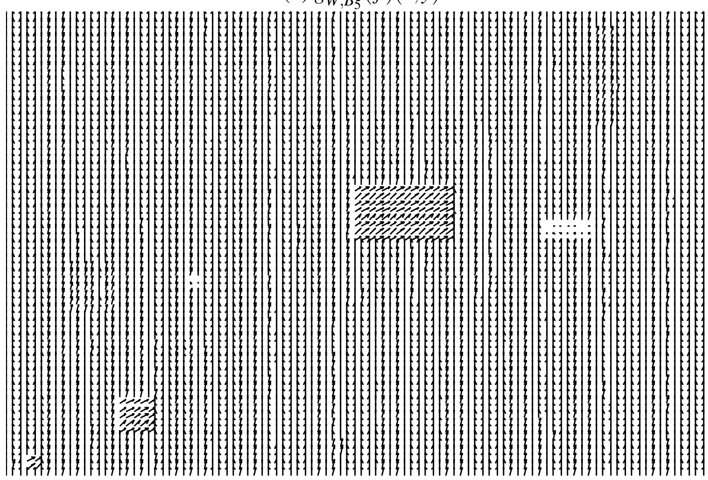

(e) $\gamma^{\circ}_{W,B_5}(f)(x,y)$

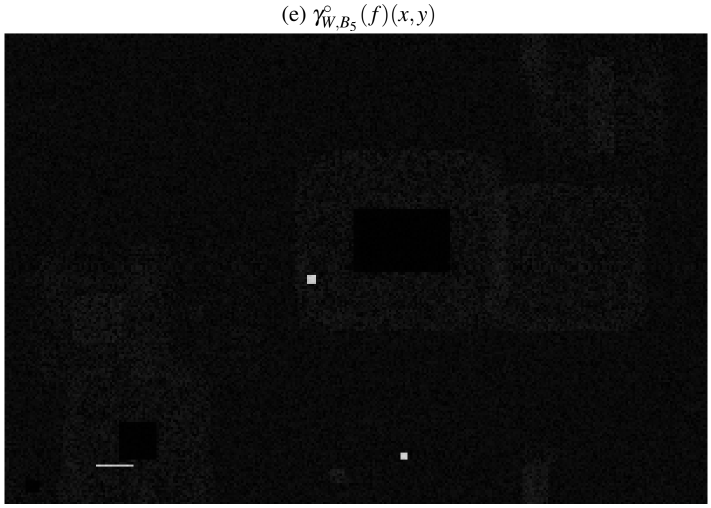

(f) $\rho^{+,\circ}_{W,B_5}(f)(x,y)$

Fig. 5 Top, examples of pseudo-dilation (b), and pseudo-erosion (c), of image $f(x,y) \in \mathbb{S}^2$, given in (a), and its derived morphological operators. Bottom, zoomed-in part of images. The structuring element B_n is a square of 5×5 pixels and W is a square of 55×55. Note that for the gradient and the top-hat images, the result is the given scalar image.